# A New Model for the FDTD Analysis of Sub-Structures on Infinite Plates

**Run Xiong[1], Bin Chen[1], Yun-Fei Mao[1, 2] and Zhao-Yang Cai[1]**

[1]National Key laboratory on Electromagnetic Environment and electro-optical Engineering
PLA University of Science and Technology. Nanjing, 210007, Jiangsu, China
xiongrun1983@hotmail.com, emcchen@163.com, myf4494@126.com, resingsun@163.com

[2]China Satellite Maritime Tracking and Control Department
Yuan Wang III, Jiangyin 214400, China

***Abstract*** ─ In this work, a new model has been proposed for the finite-difference time-domain analysis (FDTD) of sub-structure coupling problems. By stretching the total-field/scattered-field (TF/SF) boundary and the perfect electric conductor (PEC) plane into the convolution PML (CPML) layers, the coupling of sub-structures loaded on infinite planes induced by plane waves can be simulated. The validity of the proposed model has been approved from the comparison of the results obtained from the proposed model with the analytical and the open region results. The CPML performances of this model are compared in different parameters, furthermore the optimal constructive parameters of the CPML have been chosen for the high-resolution simulation of the proposed model, which can help for development of optimal sub-structure coupling.

***Index Terms*** ─ Convolution PML (CPML), Finite-difference time-domain method (FDTD), Sub-structure, Total-field/scattered-field (TF/SF)

## I. INTRODUCTION

Coupling through sub-structures (e.g., holes and seams) in conducting screens is of greater concern as the speed of the electronic designs increases [1-3]. The sub-structures may be located on conducting walls for CD-ROM's, heat vents, and input/output (I/O) cables among others. These coupling problems can be mostly simplified as one problem, which is the coupling of sub-structures located on an infinite conducting wall. Understanding the coupling mechanisms involving seams is important for estimating and reducing electro-magnetic interference.

The finite-difference time-domain (FDTD) method, which provides a simple and efficient way of solving Maxwell's equations for a variety of problems, has been widely applied in solving many types of electromagnetic coupling problems, for it has numerous time-domain and frequency-domain information.

The standard FDTD simulation with a sufficient structure resolution can be useful for analyzing the coupling mechanisms, and is frequently used as a reference to verify the subcell methods [1-5].

In [1], Wang presents a model to simulate the slot on a finite metal plate, but the truncating electric and magnetic walls wok as a waveguide and the reflection from the walls occurred. The total-field/scattered-field technique (TF/SF) [6-7] is always occupied to induce the plane wave, but it is difficult to simulate infinite scatterers illuminated by a plane wave, for the TF/SF boundary must be large enough to surround the scatterers.

In this work, a new model has been proposed for the FDTD analysis of structures on infinite planes illuminated by plane waves. The convolution perfect matched layer (CPML) [8-10] is used to truncate the computational domain. The TF/SF boundary is occupied to induce the infinite plane wave by extending the TF/SF boundary into the CPML layers. The perfect electric conductor (PEC) plate, where the sub-structure is loaded, is

*Submitted On: Apr. 11, 2012*
*Accepted On: Dec. 24, 2012*

stretched into the CPML layers to model the infinite metal plates.

In the present model, the reflection from the electric and magnetic wall of [1] can be avoided, and infinite scatterers illuminated by plane waves can be simulated without resulting in huge computational resources.

In this model, the integrality of the CPML layer is destroyed, thus the CPML performance is greatly affected, especially when the high-resolution grid is adopted. The CPML performance in this model are compared in different parameters, furthermore the optimal constructive parameters of the have been chosen for the high-resolution simulation of the proposed model, which can help for development of optimal sub-structure coupling.

## II. THE MODEL FOR THE FDTD ANALYSIS OF INFINTE PLATES

To analyze the sub-structure coupling mechanism, the PEC plane where the supposed structure is located must be large enough to eliminate the edge effect. The conventional total-field/scattered-field technique (TF/SF) [6] is always occupied to induce the plane wave, but it is difficult to illuminate infinite scatterer for the total-field region must be large enough to surround the scatter.

To overcome the shortage, we stretched both the PEC plate and TF/SF boundary into the CPML layers to simulate the infinite plate illuminated by plane waves with the minimal computational usage, as shown in Fig. 1.

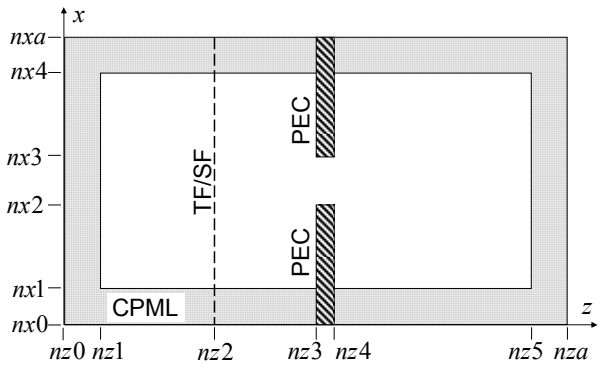


Fig. 1. The model for the FDTD analysis of sub-structures located in an infinite plate which is illuminated by a plane wave.

In this work, the CPML [8] is used to truncate the computational domain and the time-marching equation for the magnetic field component $H_y$ in the CPML can be written as

$$H_y^{n+\frac{1}{2}}(i+\tfrac{1}{2},k+\tfrac{1}{2})=\frac{2\mu-\sigma_m\Delta t}{2\mu+\sigma_m\Delta t}H_y^{n-\frac{1}{2}}(i+\tfrac{1}{2},k+\tfrac{1}{2}) - \frac{1}{\kappa_z\Delta_z}\left[E_x^n(i+\tfrac{1}{2},k+1)-E_x^n(i+\tfrac{1}{2},k)\right], + \frac{1}{\kappa_x\Delta_x}\left[E_z^n(i+1,k+\tfrac{1}{2})-E_z^n(i,k+\tfrac{1}{2})\right] + \psi_{m_{yx}}^n(i+\tfrac{1}{2},k+\tfrac{1}{2})-\psi_{m_{yz}}^n(i+\tfrac{1}{2},k+\tfrac{1}{2}) \quad (1)$$

where $\mu$ is the permeability, $\sigma_m$ is the equivalent magnetic loss, $\kappa_x$ and $\kappa_z$ are constitutive parameters, and the $\psi_{m_{yx}}$ and $\psi_{m_{yz}}$ are derived from

$$\psi_{m_{yx}}^n(i+\tfrac{1}{2},k+\tfrac{1}{2})=b_x\psi_{m_{yx}}^{n-1}(i+\tfrac{1}{2},k+\tfrac{1}{2}) + \frac{a_x}{\Delta_x}\left[E_z^n(i+1,k+\tfrac{1}{2})-E_z^n(i,k+\tfrac{1}{2})\right], \quad (2)$$

$$\psi_{m_{xz}}^n(i+\tfrac{1}{2},k+\tfrac{1}{2})=b_z\psi_{m_{xz}}^{n-1}(i+\tfrac{1}{2},k+\tfrac{1}{2}) + \frac{a_z}{\Delta_z}\left[E_x^n(i+\tfrac{1}{2},k+1)-E_x^n(i+\tfrac{1}{2},k)\right]. \quad (3)$$

The updating equation for the electric field $E_x$ in the CPML can be written as

$$E_x^{n+1}(i+\tfrac{1}{2},k)=\frac{2\varepsilon-\sigma\Delta t}{2\varepsilon+\sigma\Delta t}E_x^n(i+\tfrac{1}{2},k)-\frac{1}{\kappa_z\Delta_z} \left[H_y^{n+\frac{1}{2}}(i+\tfrac{1}{2},k+\tfrac{1}{2})-H_y^{n+\frac{1}{2}}(i+\tfrac{1}{2},k-\tfrac{1}{2})\right], -\psi_{e_{xz}}^{n+\frac{1}{2}}(i+\tfrac{1}{2},k) \quad (4)$$

where $\varepsilon$ is the permittivity, $\sigma$ is the equivalent electric loss, and

$$\psi_{e_{xz}}^{n+\frac{1}{2}}(i+\tfrac{1}{2},k)=b_z\psi_{e_{xz}}^{n-\frac{1}{2}}(i+\tfrac{1}{2},k)+\frac{a_z}{\Delta_z} \left[H_y^{n+\frac{1}{2}}(i+\tfrac{1}{2},k+\tfrac{1}{2})-H_y^{n+\frac{1}{2}}(i+\tfrac{1}{2},k-\tfrac{1}{2})\right]. \quad (5)$$

The updating equation for the electric field $E_z$ in the CPML can be written as

$$E_z^{n+1}(i,k+\tfrac{1}{2})=\frac{2\varepsilon-\sigma\Delta t}{2\varepsilon+\sigma\Delta t}E_z^{n}(i,k+\tfrac{1}{2})+\frac{1}{\kappa_x\Delta_x}\left[H_y^{n+\frac{1}{2}}(i+\tfrac{1}{2},k+\tfrac{1}{2})-H_y^{n+\frac{1}{2}}(i-\tfrac{1}{2},k+\tfrac{1}{2})\right]+\psi_{e_{zx}}^{n+\frac{1}{2}}(i,k+\tfrac{1}{2}) \quad (6)$$

where

$$\psi_{e_{zx}}^{n+\frac{1}{2}}(i,k+\tfrac{1}{2})=b_x\psi_{e_{zx}}^{n-\frac{1}{2}}(i,k+\tfrac{1}{2})+\frac{a_x}{\Delta_x}\left[H_y^{n+\frac{1}{2}}(i+\tfrac{1}{2},k+\tfrac{1}{2})-H_y^{n+\frac{1}{2}}(i-\tfrac{1}{2},k+\tfrac{1}{2})\right] \quad (7)$$

The coefficient $a$ and $b$ can be obtained from

$$b_i=exp\left[-(\frac{\sigma_i}{\kappa_i}+\alpha_i)\frac{\Delta t}{\varepsilon_0}\right],\quad i=x,z, \quad (8)$$

$$a_i=\frac{\sigma_i}{\sigma_K\kappa_i+\kappa_i^2\alpha_i}\left[\exp\left(-(\frac{\sigma_i}{\kappa_i}+\alpha_i)\frac{\Delta t}{\varepsilon_0}\right)-1\right],\ i=x,z. \quad (9)$$

Within the CPML layers, the constitutive parameters are scaled using polynomial scaling [12]:

$$\sigma(\rho)=\sigma_{max}(\rho/D)^m, \quad (10)$$

$$\kappa(\rho)=1+(\kappa_{max}-1)(\rho/D)^m, \quad (11)$$

$$\alpha(\rho)=\alpha_{max}(1-\rho/D)^m, \quad (12)$$

where $\rho$ indicates the distance from the air-CPML interface into the CPML layer, $D$ is the depth of the CPML, and $m$ is the order of the polynomial and is chosen to be 4 in this work. The choice for $\sigma_{max}$ suggest in [13] is expressed as

$$\sigma_{opt}=\frac{m+1}{150\pi\Delta_i},\quad i=x,z, \quad (13)$$

where $\Delta_i$ is the grid spacing along the $x$ and $z$ axis.

To simulate a seam located in an infinite plate, we extended the PEC wall into the CPML layers, shown as the hatching areas in Fig. 1, which is:

$$E_x(x,nz3:nz4)=\begin{cases}E_x(x,nz3:nz4), & x\in(nx2,nx3)\\ 0, & x\in(nx0,nx2)\cup(nx3,nxa)\end{cases} \quad (14)$$

Note that some segments of the PEC plates lie in the CPML region.

The TF/SF technique is extensively used to induce the plane wave, but TF/SF connecting surface is always a closed surface and the scatterer is fully imbedded in the total field region, as shown in [6, Fig. 2]. Therefore, to simulate the plane wave illuminating the infinite PEC plate, one has to use a very large total-field domain to embed the plate, which will result in huge memory usage, especially when high-resolution simulation is involved.

In this work, the TF/SF boundary is stretched into the CPML layer to induce a plane wave illuminating an infinite PEC plate, shown as the dashed line in Fig. 1. Therefore, the connecting surface has only one face and the FDTD updating equations at the boundary can be written as:

$$H_y^{n+\frac{1}{2}}(x,nz2-\tfrac{1}{2})=H_y^{n+\frac{1}{2}}(x,nz2-\tfrac{1}{2})_{FDTD}+\frac{\Delta t}{\mu\Delta_z}E_{x,i}^{n}(nz2),\ \ x\in(nx0,nxa) \quad (15)$$

$$E_x^{n+1}(x,nz2)=E_x^{n+1}(x,nz2)_{FDTD}+\frac{\Delta t}{\varepsilon\Delta_z}H_{y,i}^{n+\frac{1}{2}}(nz2-\tfrac{1}{2}),\ \ x\in(nx0,nxa) \quad (16)$$

It is worth to note that the TF/SF boundary dimension in the $x$ direction of both the $E_x$ and $H_y$ are from *nx0* to *nxa*, which is from the down CPML edge to the up CPML edge.

When the incidence of oblique propagation directions is involved, the generalized TF/SF (G-TF/SF) [11] technique is used.

$$\psi_{inc}^{num}=X_0^{num}A_{PML}(\theta_{inc},\xi_x,\xi_y). \quad (17)$$

Here, $\psi_{inc}^{num}$ represents the required incident $E_{x,i}^{n}$ or $H_{y,i}^{n+\frac{1}{2}}$ field component in (15) and (16) in the CPML region. $X_0^{num}$ is the corresponding free space incident field. $A_{PML}(\theta_{inc},\xi_x,\xi_y)$ is the appropriate multiplying factor at the observation point in the CPML region, where: $\theta_{inc}$ is the incident angle of the plane wave; $\xi_x=d_x\zeta_{x,PML}$; $\xi_z=d_z\zeta_{z,PML}$; $\zeta_{x,PML}$ and $\zeta_{z,PML}$ are the electric or magnetic loss constants at the observation point in the CPML region in the $x$ and $z$ directions, respectively; and $d_x$ and $d_z$ are the depths of the observation point inside the CPML region in the $x$ and $z$ directions, respectively. $A_{PML}(\theta_{inc},\xi_x,\xi_y)$ can be derived from [11] for the up and down CPML areas respectively.

The segments of the TF/SF boundary and the PEC plates that lie in free space are treated exactly like the conventional TF/SF [6] boundary and PEC plates. While in the CPML regions, special treatment are needed. The flowchart of the field update in the CPML regions is shown in Fig. 2. For other regions, the conventional time-marching equations can be useful.

There is a key advantage to this methodology, that the area at the right side of the TF/SF boundary is the entire total field region. Therefore, only a limited computational domain can model the infinite scatterer illuminated by an infinite plane wave.

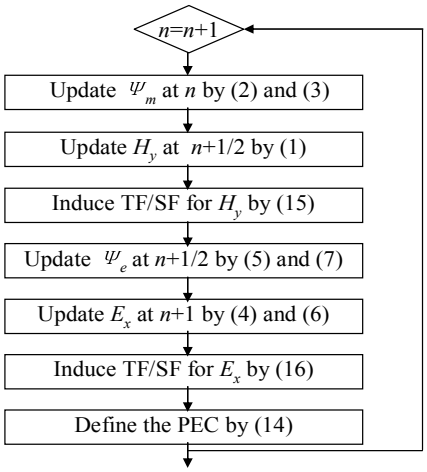


Fig. 2. Flowchart of field in the CPML region.

## III. NUMERICAL VALIDATION OF THE PROPOSED ODEL

### A. Validation of the proposed TF/SF boundary

In this section, numerical examples are implemented to validate the TF/SF boundary of the proposed model. The computational domain is shown in Fig. 3, where the PEC plane is removed. The TF/SF boundary is set to be 12 cells away from the left air-CPML interface, and 28 cells from the right air-CPML interface. The computational domain is 25 cells from the up air-CPML interface to the down interface. The computational domain is truncated along the *x*- and *z*-directions by 10 additional CPML layers, which results in a 45×60 cells lattice. The electric field component $E_x$ is monitored at the center of the reference plane, which is 16 cells away from the TF/SF boundary.

The sinusoidal modulated Gaussian pulse is excited as the normal incident pulse

$$E_x(t)=\exp\left[-4\pi\left(\frac{t-T_c}{T_d}\right)^2\right]\sin\left[2\pi f_c\left(t-T_c\right)\right], \quad (18)$$

where $f_c$=1 GHz, $T_d=2/f_c$, $T_c=0.6T_d$.

The source is induced through the proposed TF/SF boundary (15) and (16), where *nz*2=22. Square cells are used, with the grid size Δ=1 cm, and the time step is $\Delta t=\Delta/2c$, where *c* is the speed of light in the free space.

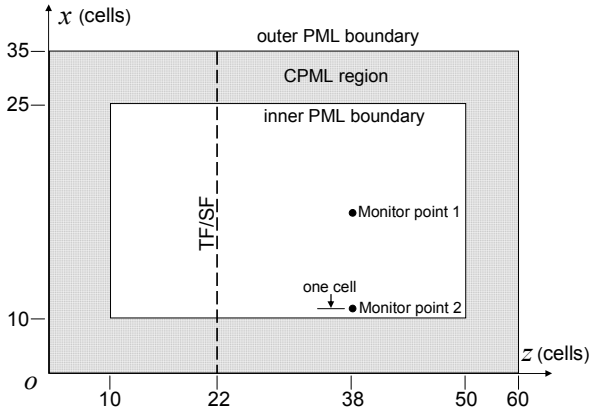


Fig. 3. Computational domain.

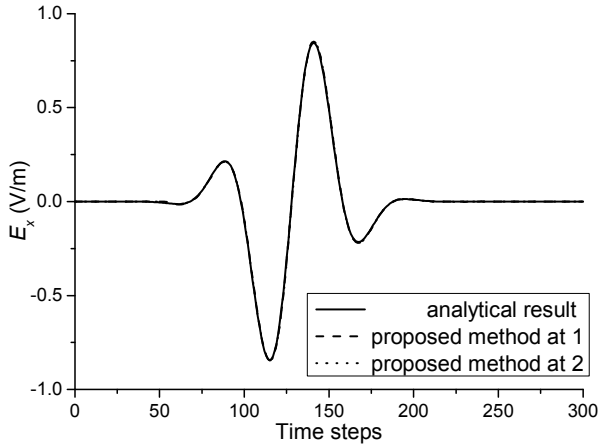


Fig. 4. Comparison of the electric field component got from the proposed method with analytical result.

To verify the validity of the proposed TF/SF boundary, which is stretched into the CPML layers, the electric field component at the two monitor points is compared with the analytical result. The reference Point 1 is at the center of the plane 16 cells from the TF/SF boundary, and the Point 2 is one cell from the down air-CPML interface.

Figure 4 plots the waveforms calculated at the two points, where the analytical result is also presented as a benchmark. It is clear that the fields predicted by the proposed method are in good agreement with the analytical result. Comparison

of the fields at other positions indicates the same conclusion.

### B. Validation of the proposed PEC boundary

In this section, numerical examples are implemented to validate the proposed PEC boundary, which is stretched into the CPML layers. The computational domain is the same as Fig. 3, where the PEC plate is set to be 12 cells from TF/SF boundary and 15 cells from the right CPML interface, and the PEC plate is 1 cell thick. The slot, which is 1 cell wide, is located at the center of the PEC plate. Other conditions are the same as the above section.

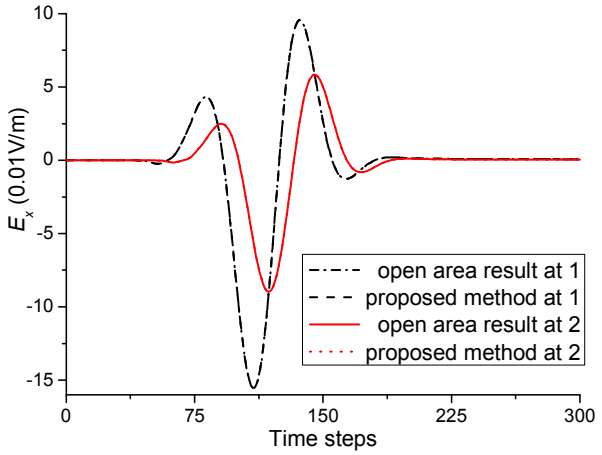


Fig. 5. Waveforms of the electric field component $E_x$ as computed from the proposed model and the open area results.

To provide a benchmark for comparison, an open area result is needed. To this end, the same mesh is extended by 150 cells in the $x$ and $z$ dimensions, leading to a 340×350 cells lattice. We compared the electric field component as computed from the proposed model and that from the reference solution, showing a very good mutual agreement at both the two measure points, as shown in Fig. 5.

## IV. CPML PARAMETERS FOR THE HIGH-RESOLUTION SIMULATION

When the FDTD method is adopted to analyze the sub-structure coupling, the grid dimension is always chosen to be small compared with the supposed structure size (e.g., $w$/15 or $d$/15, where $w$ and $d$ are the slot width and depth respectively), in order to satisfy the precision demand on the slot resolution [2]. It can be seen from Figs. 4-5 that the CPML performance is excellent with the ordinary resolution, but the CPML performance with high-resolution has not been analyzed. In the present model, the integrality of the CPML layer is destroyed, thus the CPML performance is greatly affected, especially when the high-resolution grid is adopted.

To check the CPML performance of the proposed model, the computational domain shown in Fig. 6 is adopted, where the configuration is also shown. The source of (18) is chosen to be the incident pulse, and square FDTD cells are adopted with the size Δ=0.3 mm. The depth of the slot plate is 20 cells. The slot, which is located at the centre of plate, is 15 cells wide. 10-cell-thick CPML layers terminate the grid, which results in a 55×166 cells lattice.

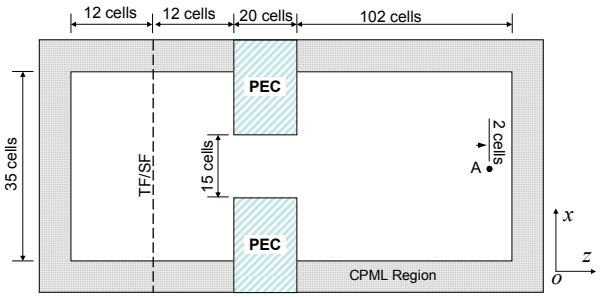


Fig. 6. Computational domain of the 2-D structures, where the observation point is 2 cells from the CPML boundary.

To study the reflection error due to the CPML in this model, a reference problem is also simulated. The same mesh is extended by 4500 cells in the $x$ and $z$ dimensions, leading to a 9055×9166 cells lattice. The fields within the lattice are then excited by an identical source, and the time-dependent fields are recorded within the region representing the original lattice. The error relative to the reference solution (in decibels) is computed as a function of time using:

$$R_{dB} = 20\log_{10}\frac{\left|E_x^R(t) - E_x^T(t)\right|}{max\left|E_x^R(t)\right|}, \qquad (19)$$

where $E_x^T(t)$ represents the field computed in the test domain and $E_x^R(t)$ is the reference field computed using the larger domain.

There are literatures about the parameters of

the CPML [8], [12]. In [8], $\kappa_{max}$=5, $\sigma_{max}/\sigma_{opt}$=1.3, and $\alpha$ varies in the CPML layers with $\alpha_{max}$=0.05. In [12], $\kappa_{max}$=25, $\sigma_{max}/\sigma_{opt}$=1.6, while $\alpha$=0.003 and is held constant through the CPML layers. The reflective error of the CPML with the two parameters at the measurement Point *A*, which is 2 cells (0.6 mm) away from the CPML interface computed via (19) is recorded, as shown in Fig. 7. It is shown that the reflection error can reach as large as -50 dB for this case when the CPML is adopted with the parameters of [8] and [12].

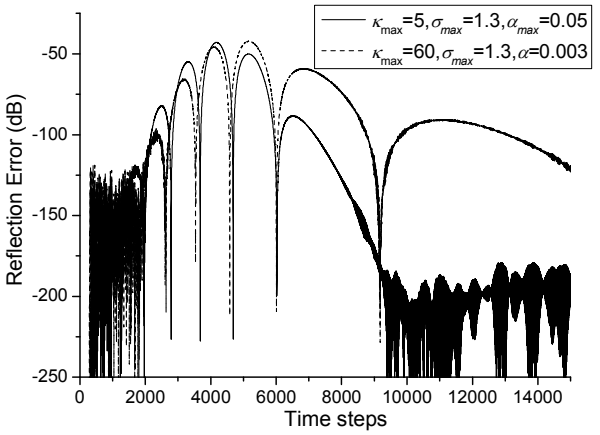


Fig. 7. Error in the electric field intensity relative to the field's maximum amplitude versus time for the CPML of the parameters of [8] and [12].

To get a better CPML performance, the $\alpha_i$ is chose to decrease to zero away from the boundary interface as (12), and the relative reflection error is calculated via (19) with varied CPML constitutive parameters. Figure 8 plots contours of the maximum relative error in dB as a function of $\kappa_{max}$ and $\sigma_{max}/\sigma_{opt}$ at Point A, with $\alpha_{max}$=1.25. It can be seen that the maximum relative reflection error as low as -115 dB is achieved by selecting $\kappa_{max}$=40, $\sigma_{max}/\sigma_{opt}$=0.9 and $\alpha_{max}$=1.25.

## V. VALIDATION THE POPOSED MODEL IN 3-D PROBLEMS

To verify the proposed model with the supposed constitutive parameters, the three-dimensional slot-coupling problem is included, and the computational domain is shown in Fig. 9. The depth of the slot plane is 2 mm, and the conducting wall is introduced by the supposed PEC boundary. The size of the slot, which is located at the center of the conducting wall, is $L\times w$=150×1 mm. The slot plane is illuminated by a normal incidence, and the pulse in [14] is excited through the supposed TF/SF boundary

$$E_x^{inc}(t)=\frac{1}{0.8258}\frac{1}{e^{[-20(t-t_0)/\beta]}+e^{[(t-t_0)/\beta]}}, \qquad (20)$$

where $t_0$=6.67×10$^9$, and $\beta$=6.67×10$^9$.

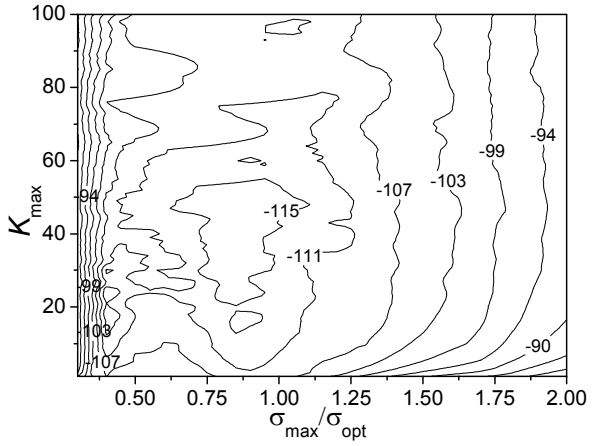


Fig. 8. Maximum relative error at Point A as a function of $\kappa_{max}$ and $\sigma_{max}/\sigma_{opt}$ (with D=10 cells, $\alpha_{max}$=1.25 and $m$=4)

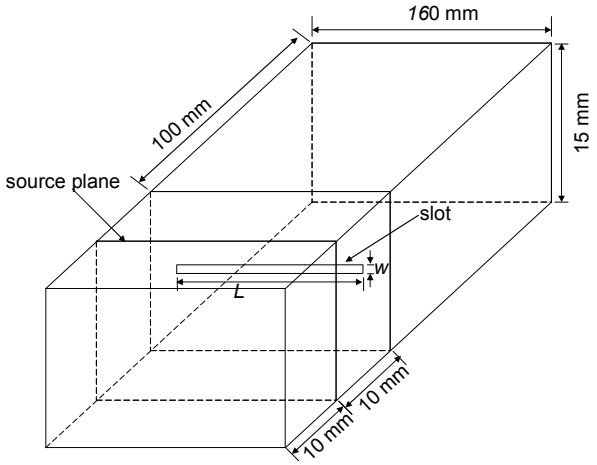


Fig. 9. Computational domain of the three-dimensional slot coupling.

Cubic FDTD cell is used, and the spatial step is 1/11 mm, while the time step is 0.06 ps. The computational domain is truncated by a 10-cell layer CPML, and the problem is simulated with the CPML parameters of [8], [12] and this study. The penetrating electric field component is monitored at the center of the reference plane, which is 90 mm away from the slot plane at the

shadow side.

Figure 10 shows the waveforms of the electric field at the observation point. It can be seen that obvious reflections from the CPML occurred for the constitutive parameters given by [8] and [12], while the CPML performs well with the constitutive parameters in this work.

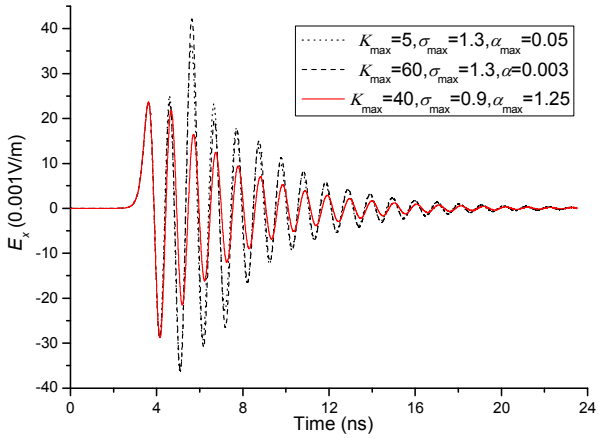


Fig. 10. Waveforms of the penetrating electric field component $E_x^p$ calculated by the proposed model with the constitutive parameters of [8], [12], and this study.

## VI. CONCLUSIONS

In this work, a new model has been proposed for the high-resolution FDTD analysis of sub-structures on the infinite plates induced by plane waves. The CPML is used to truncate the computational domain. The PEC plate, where the sub-structure is loaded, is stretched into the CPML to model the infinite plane. The TF/SF boundary is occupied to induce the plane wave illuminating the infinite PEC by extending the TF/SF boundary into the CPML layers.

It has been approved that the set of the TF/SF boundary and the PEC boundary in the proposed model are numerically efficient. The CPML performances are compared in different parameters, furthermore the optimal constructive parameters of the CPML have been chosen for the high-resolution simulation of the proposed model, which can help for development of optimal sub-structure coupling. Three-dimensional slot coupling results are also used to verify the efficiency of the proposed model with the supposed parameters.

The present model can be used for the high-resolution FDTD analysis of the sub-structure coupling located on infinite conducting walls illuminated by plane waves.

## REFERENCES

1. B.-Z. Wang, “Enhanced Thin-Slot Formalism for the FDTD Analysis of Thin-Slot Penetration,” *IEEE Microw. Guided Wave Lett.*, vol. 5, pp. 142-143, May 1995.
2. M. A. Gkatzianas, C. A. Balanis and R. E. Diaz, “The Gilbert–Holland FDTD Thin Slot Model Revisited: an Alternative Expression for the In-Cell Capacitance,” *IEEE Microw. Wireless Compon. Lett.*, vol. 14, pp. 219-221, May 2004.
3. D. W. Sun, J. H. Yu, “Extending the 2-D Contour Path Method to the 3-D,” *Applied Computational Electromagnetics Society (ACES) Journal*, vol. 10, pp. 655-657, 2011.
4. R. Xiong, B. Chen, Q. Yin and Z.-Y. Cai, “Improved Formalism for the FDTD Analysis of Thin-Slot Penetration by Equivalence Principle,” *IEEE Antennas and Wireless Propag. Lett.*, vol. 10, pp. 655-657, 2011.
5. C. M. Ruiz, J. J. Simpson, “Ultra High-Resolution FDTD Modeling of a High-Performance VLSI Package for Identifying Resonances and Coupling,” *Applied Computational Electromagnetics Society (ACES) Journal*, vol. 26, no. 4, pp. 284-294, April 2011.
6. K. Umashankar, A. Taflove, "A Novel Method to Analyze Electromagnetic Scattering of Complex Objects," *IEEE Trans. Electromag. Compat.*, vol. EMC-24, no. 4, pp. 397-405, Nov. 1982.
7. H. A. Abdallah, “An Optimized High-Order Implicit FDTD Solver with One-Sided TF/SF for Simulation of Photonic Devices,” *Applied Computational Electromagnetics Society (ACES) Journal*, vol. 20, no. 1, pp. 78-85, March 2005.
8. J. A. Roden, and S. D. Gedney, “Convolution PML (CPML): an Efficient FDTD Implementation of the CFS-PML for Arbitrary Media”, *Microwave and Opt. Technol. Lett.*, vol. 27, no. 5, pp. 334-339, Dec. 2000.
9. N. Okada, J. B. Cole, “Nonstandard Finite Difference Time Domain Algorithm for Berenger’s Perfectly Matched Layer,” *Applied Computational Electromagnetics Society (ACES) Journal*, vol. 26, no. 2, pp. 153-159, February 2011.
10. M. Wong, A. R. Sebak, “The Floating PML Applied to Practical FDTD Applications,” *Applied Computational Electromagnetics Society (ACES) Journal*, vol. 23, no. 2, pp. 110-119, June 2008.
11. V. Anantha and A. Taflove, "Efficient Modeling of Infinite Scatterers using a Generalized Total-Field/Scattered-Field FDTD Boundary Partially Embedded within PML," *IEEE Trans.*

*Antennas. Propagat.*, vol. 39, no. 2, pp. 147-155, May 2002.

12. Z.-Y. Cai, B. Chen, K. Liu, Y.-T. Duan, and Y.-F. Mao, "The CFS-PML for Periodic Laguerre-Based FDTD Method," *IEEE Microw. Wireless Compon. Lett.*, vol. 22, no. 4, pp. 487-489, 2012.
13. A. Taflave and S. C. Hagness, *Computational Electrodynamics: The Finite-Difference Time-Domain Method*, 2nd ed, Boston, Artech House, 175-134, 2000.
14. K.-P. Ma, M. Li, J. L. Drewniak, T. H. Hubing and T. P. V. Doren, "Comparison of FDTD Algorithms for Subcellular Modeling of Slots in Shielding Enclosures," *IEEE Trans. Electro*mag. Compat., vol. 39, no. 2, pp. 147-155, May 1997.

**Run Xiong** was born in Sichuan province, China, in 1983. He received the B.S. and M.S. degrees in electric systems and automation from Engineering Institute of Corps of Engineers, PLA University of Science and Technology, Nanjing, China, in 2005 and 2010 respectively, where he is currently working toward the Ph.D. degree. He is now with the National Key laboratory on Electromagnetic Environment and electro-optical Engineering, and his research interests include computational electromagnetics and EMC.

**Bin Chen** was born in Jiangsu, China, in 1957. He received the B.S. and M.S. degrees in electrical engineering from Beijing Institute of Technology, Beijing, China, in 1982 and 1987, respectively, and the Ph.D. degree in electrical engineering from Nanjing University of Science and Technology, Nanjing, China, in 1997. Currently, he is a Professor at National Key laboratory on Electromagnetic Environment and electro-optical Engineering, PLA University of Science and Technology. His research includes computational electromagnetics, EMC and EMP.

**Yunfei Mao** was born in Zhejiang province, China, in 1984. He received the B.S. degrees in electric systems from Engineering Institute of Corps of Engineers, PLA University of Science and Technology, Nanjing, China, in 2006 and 2009 respectively, where he is currently working toward the Ph.D. degree. He is now with the National Key laboratory on Electromagnetic Environment and electro-optical Engineering. His research interests include computational electromagnetics.

**Zhaoyang Cai** was born in Henan province, China, in 1985. He received the B.S. degrees in electric systems from Engineering Institute of Corps of Engineers, PLA University of Science and Technology, Nanjing, China, in 2007 and 2011 respectively, where he is currently working toward the Ph.D. degree. He is now with the National Key laboratory on Electromagnetic Environment and electro-optical Engineering. His research interests include computational electromagnetics.